Ferroelectrics, 483: 75–85, 2015

ISSN: 0015-0193 print / 1563-5112 online
DOI: 10.1080/00150193.2015.1058690

Taylor & Francis
Taylor & Francis Group

Theoretical Modelling of the Energy Surface (001) and Topology of $CaZrO_3$ Perovskite

ROBERTS I. EGLITIS*

Institute of Solid State Physics, University of Latvia, 8 Kengaraga Str., Riga LV 1063, Latvia

I present the results of ab initio *calculations of surface relaxations, rumplings, energetics, optical band gaps, and charge distribution for the $CaZrO_3$ (001) surfaces using computer code CRYSTAL and a hybrid description of exchange and correlation. I consider both CaO and ZrO_2-terminations of the $CaZrO_3$ (001) surface. On the both CaO and ZrO_2-terminated $CaZrO_3$ (001) surfaces, I find that all upper and third layer atoms relax inwards, whereas all second layer atoms relax upwards. I predict a considerable increase of the Zr-O chemical bond covalency (0.102*e*) near the ZrO_2-terminated $CaZrO_3$ (001) surface relative to the $CaZrO_3$ bulk (0.086*e*). My calculated CaO (0.87 eV) and ZrO_2-terminated (1.33 eV) $CaZrO_3$ (001) surface energies are considerably smaller than another ABO_3 perovskite polar (011) and (111) surface energies. The calculated optical band gaps near the CaO (5.00 eV) and ZrO_2-terminated (5.22 eV) CaZrO3 (001) surfaces are considerably reduced with respect to the bulk band gap (5.40 eV).*

Keywords *Ab initio* calculations; (001) surfaces; $CaZrO_3$; B3LYP

I. Introduction

Ab initio calculations of ABO_3 perovskite surface characteristics are important in order to understand processes in which surfaces play a key role, such as the chemistry of surface reactions, interface phenomena, and adsorption [1–5]. In view of this ABO_3 perovskite material industrial importance, it is surprising that there have been only one theoretical study of $CaZrO_3$ (001) surface atomic and electronic structure performed recently by Brik *et al*. [6]. However, a huge number of first principles studies of another ABO_3 perovskite (001) surfaces have been recently reported [1, 2, 7–21]. It is well known that the perovskite oxides, as well as their forming simple oxides, are highly resistant against particle radiation [22, 23], while their surfaces do not show similar resistance [24]. Recently it was demonstrated, that alkaline earth metal zirconates are also promising surface modified hybrid composite materials with excellent magnetic, luminescent and conductive functions [25, 26].

There are no experimental studies reported dealing with $CaZrO_3$ surfaces, but a large amount of experimental studies of $SrTiO_3$ (001) surfaces have been performed [27–32]. For example, Bickel *et al*. [27] investigated the (001) surface structure of SrTiO3 at

Received October 2, 2014; in final form April 14, 2015.
*Corresponding author. E-mail: rieglitis@gmail.com
Color versions of one or more of the figures in the article can be found online at www.tandfonline.com/gfer.

$T = 120$ K by means of low-energy-electron diffraction (LEED). They got the best theory-experiment fit results for a surface containing domains of two different layer terminations. Four years later, Hikita *et al*. [28] experimentally studied the electronic and atomic structure of TiO_2 and SrO-terminated $SrTiO_3$ (001) surface using reflection high energy electron diffraction (RHEED), X-ray photoelectron spectroscopy (XPS) and UPS. According to the results of Hikita *et al*., the oxygen atoms on the outermost $SrTiO_3$ surface are pulled out for 0.10 Å and 0.16 Å, respectively. It is important to notice, that the LEED and RHEED experiments contradict each other in the sign of the near-surface interplanar separation between the first and the second surface plane Δd_{12} for SrO-terminated $SrTiO_3$ (001) surface. Ikeda *et al*. [29] determined the surface relaxation and rumpling of TiO_2-terminated $SrTiO_3$ (001) surface by means of medium energy ion scattering (MEIS). Charlton *et al*. [30] used the X-ray diffraction in order to determine the 300 K structure of $SrTiO_3$ (001) 1×1 with a termination of 78% TiO and 22% of SrO. The data of Charlton *et al*. indicated that a lateral ferroelectric distortion was absent on both terminations. Van der Heide *et al*. [31] analyzed the chemical and structural properties of several $SrTiO_3$ (001) surfaces prior to and following UHV and O_2 annealing using XPS, time-of-flight and recoiling spectrometry (TOF-SARS), and LEED. The simulations of the TOF-SARS azimuthal scans indicated that the O atoms are located 0.1 Å above the Ti-terminated surface layer. Finally, Maus-Friedrichs *et al*. [32] investigated the $SrTiO_3$ (001) surface with the metastable impact electron spectra (MIES) and ultraviolet photoelectron spectroscopy (UPS) methods.

The paper is structured as follows. Section II describes the details of current computational calculations dealing with $CaZrO_3$ (001) surfaces. The main part of the paper is formed by Section III, which presents the *ab initio* calculation results dealing with $CaZrO_3$ (001) surface relaxations, rumplings, energetics, optical band gaps and charge distribution. The current calculation results are compared with the relevant experimental and computational data available in the literature. Finally, the conclusions are summarized in Section IV.

II. Computational Details

Ab initio calculations in the framework of DFT using the CRYSTAL computer code [33] have been performed for $CaZrO_3$ (001) surfaces. Unlike the plane-wave codes employed in many previous ABO_3 perovskite (001) surface studies, [34, 35] CRYSTAL uses localized Gaussian-type Basis Sets (BS). In calculations by Piskunov *et al*. [36], the BSs were developed for $SrTiO_3$, $BaTiO_3$ and $PbTiO_3$. The CRYSTAL BS are believed to be largely transferable, so that, once determined for some chemical constituent, they may be successfully applied in the calculations for a wide variety of chemical substances, for example SrF_2, BaF_2 and CaF_2 [37–42], where the latter participates. The numerical calculations in this paper were performed using the hybrid exchange-correlation B3LYP functional involving a hybrid of nonlocal Fock exact exchange, LDA exchange and Becke's gradient corrected exchange functional [43], combined with the nonlocal gradient corrected correlation potential by Lee-Yang-Parr [44].

The reciprocal space integration was performed by sampling the Brillouin zone of the five atom cubic $CaZrO_3$ unit cell with the $5 \times 5 \times 5$ Pack-Monkhorst net [45], that provides the balanced summation in direct and reciprocal spaces. To achieve high accuracy, large enough tolerances of 7, 8, 7, 7, 14 were chosen for the Coulomb overlap, Coulomb penetration, exchange overlap, the first exchange pseudo-overlap, and for the second exchange pseudo-overlap, respectively [33].

The $CaZrO_3$ (001) surfaces were modeled with two-dimensional slabs consisting of several planes perpendicular to the [001] crystal direction. The CRYSTAL code allowed to avoid artificial periodicity along the *Oz* direction and to perform simulations for stand-alone two-dimensional slabs. To calculate $CaZrO_3$ (001) surfaces, symmetrical slabs consisting of nine alternationg CaO and ZrO_2 layers were used. One of these slabs was terminated by CaO planes and consisted of a supercell containing 22 atoms (see Fig. 1). The second slab was terminated by ZrO_2 planes and consisted of a supercell containing 23 atoms (see Fig. 2). These slabs are non-stoichiometric, with unit cell formulae $Ca_5Zr_4O_{13}$ and $Ca_4O_5O_{14}$, respectively.

In order to calculate the $CaZrO_3$ (001) surface energy, I started with the cleavage energy for unrelaxed CaO- and ZrO_2-terminated $CaZrO_3$ (001) surfaces. Surfaces with both terminations simultaneously arise under (001) cleavage of the crystal, and I adopt the convention that the cleavage energy is equally distributed between the created surfaces. In my calculations, the nine-layer CaO-terminated (001) slab with 22 atoms and the ZrO_2-terminated one with 23 atoms represent, together, nine bulk unit cells (45 atoms) so that

$$E_{surf}{}^{unr}(\xi) = \tfrac{1}{4}[E_{slab}{}^{unr}(CaO) + E_{slab}{}^{unr}(ZrO_2) - 9E_{bulk}], \quad (1)$$

where ξ denotes CaO or ZrO_2, $E_{surf}{}^{unr}(\xi)$ are the unrelaxed energies of CaO- or ZrO_2-terminated $CaZrO_3$ (001) slabs, E_{bulk} is the energy per bulk unit cell, and the factor of $\frac{1}{4}$ comes from the fact that I create four surfaces upon the crystal cleavage procedure. Next, I can calculate the relaxation energies for each of CaO and ZrO_2 terminations, when both sides of the slabs relax, according to

$$E_{rel}(\xi) = \tfrac{1}{2}\left[E_{slab}{}^{rel}(\xi) - E_{slab}{}^{unr}(\xi)\right], \quad (2)$$

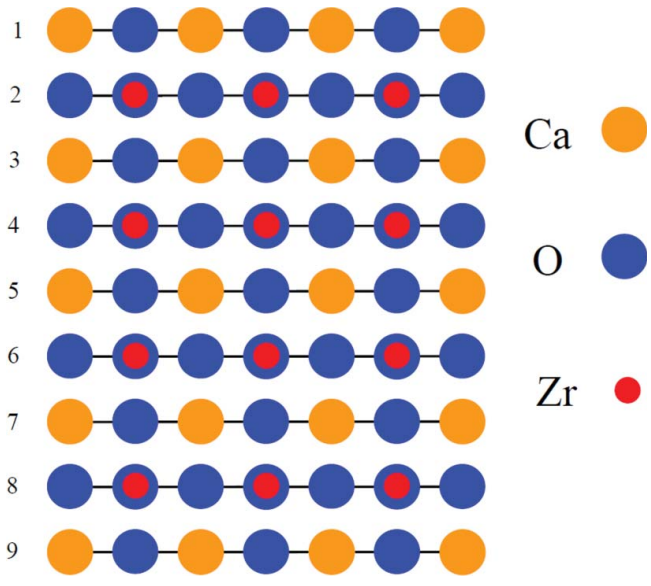

Figure 1. Side view of CaO-terminated $CaZrO_3$ (001) surface containing nine layers.

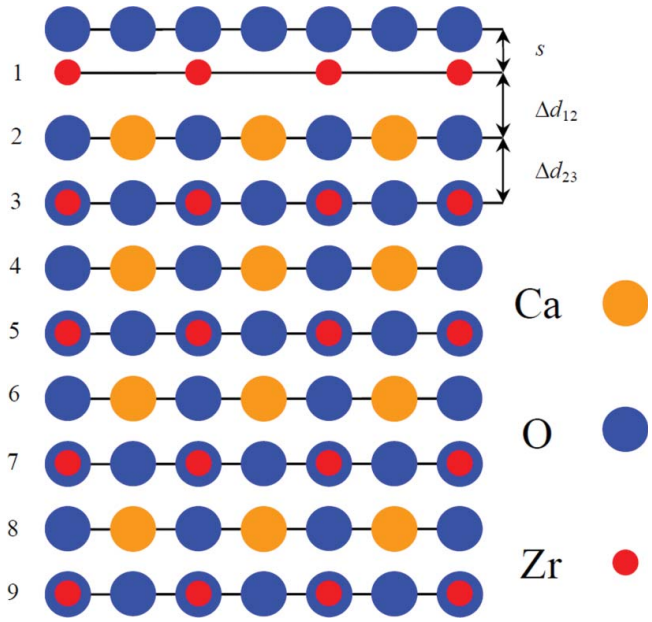

Figure 2. Side view of a ZrO_2-terminated $CaZrO_3$ (001) surface with the definitions of the surface rumpling s and the near-surface interplane distances Δd_{12} and Δd_{23}, respectively.

where $E_{slab}{}^{rel}(\xi)$ is the slab energy after relaxation (and again ξ = CaO or ZrO_2). The surface energy is then defined as a sum of the cleavage and relaxation energies,

$$E_{surf}(\xi) = E_{surf}{}^{unr}(\xi) + E_{rel}(\xi). \quad (3)$$

III. Main Calculation Results

As a starting point for my calculations, I calculated the $CaZrO_3$ bulk lattice constant 4.157 Å (see Table 1). The experimentally measured $CaZrO_3$ bulk lattice constant is equal to 4.020 Å [46]. To characterize the chemical bonding and covalency effects, I used a standard Mulliken population analysis for the effective atomic charges Q and other local properties of electronic structure as described, for example, in [47, 48].

My calculated bulk effective charges are $(+1.787e)$ for the Ca atom, $(+2.144e)$ for the Zr atom, and $(-1.310e)$ for the O atom (see Table 2). The calculated bond population of the chemical bonding between Zr and O atoms is $(0.086e)$, but bond populations

Table 1
The calculated lattice constant (in Å) for the $CaZrO_3$ bulk using the hybrid B3LYP method. The experimental bulk lattice constant [46] is listed for comparison

Material	Calculated lattice constant	Experim. lattice constant
$CaZrO_3$	4.157	4.020

Table 2
Calculated effective charges Q and bond populations P (in e) for bulk $CaZrO_3$

$CaZrO_3$		
Ion or bond	Property	Value
Ca	Q	+1.787
O	Q	−1.310
Zr	Q	+2.144
Ca-O	P	+0.014
Zr-O	P	+0.086
O-O	P	−0.010

between O and O atoms is negative ($-0.010e$), which indicates repulsion between O-O atoms. The bond population between Ca and O atoms is considerable smaller, only ($+0.014e$) than, for example, between Zr and O atoms.

The $CaZrO_3$ atomic displacements calculated by me using the B3LYP method for CaO- and ZrO_2-terminated $CaZrO_3$ (001) surfaces are shown in Tables 3 and 4. According to the results my calculations, all atoms of the first $CaZrO_3$ surface layer relax inwards, i.e. towards the bulk, for both CaO- and ZrO_2-terminated $CaZrO_3$ (001) surfaces. The outward relaxation of all atoms in the second layer is found for both terminations of the $CaZrO_3$ (001) surface. The largest calculated relaxation between all atoms is for the CaO-terminated $CaZrO_3$ (001) surface upper layer Ca atom, which moves inwards by 10.01% of the lattice constant a_0.

In order to make it possible to compare the calculated surface structures with further experimental data, the surface rumpling s (the relative displacement of oxygen with respect to the metal atom in the surface layer) (see Figures 1 and 2) and the changes in interlayer distances Δd_{12} and Δd_{23} (1, 2, and 3 are the numbers of near-surface layers) are presented in Table 5. My calculations of the interlayer distances are based on the positions of relaxed metal ions, which are known to be much stronger electron scatterers than oxygen ions [27]. As it is possible to see from Table 5 both CaO- and ZrO_2-terminated $CaZrO_3$ (001) surfaces show the reduction of interlayer distance Δd_{12} and expansion of

Table 3
Atomic relaxation of the uppermost three layers (in percent of lattice constant $a_0 = 4.157$ Å) for the CaO-terminated $CaZrO_3$ (001) surface calculated by the hybrid B3LYP method. Positive (negative) values refer to displacements in the direction outwards from (inwards to) the surface

Layer Number	Ion	B3LYP (Δz % of a_0)
1	Ca	−10.01
	O	−0.79
2	Zr	+1.11
	O	+0.01
3	Ca	−2.60
	O	−0.48

Table 4

Atomic relaxation of the uppermost three layers (in percent of lattice constant $a_0 = 4.157$ Å) for the ZrO_2-terminated $CaZrO_3$ (001) surface calculated by the hybrid B3LYP method. Positive (negative) values refer to displacements in the direction outwards from (inwards to) the surface

Layer number	Ion	B3LYP (Δz % of a_0)
1	Zr	−1.30
	O	−2.31
2	Ca	+4.23
	O	+1.25
3	Zr	−0.05
	O	−0.09

Table 5

The calculated surface rumpling s and relative displacements (Δd_{ij}) for the three near-surface planes of CaO- and ZrO_2-terminated $CaZrO_3$ (001) surface (in per cent of bulk lattice constant)

CaO-terminated				ZrO_2-terminated		
Method	s	Δd_{12}	Δd_{23}	s	Δd_{12}	Δd_{23}
B3LYP	9.22	−11.12	+3.71	1.01	−5.53	+4.28

Table 6

Calculated absolute magnitudes of atomic displacements D (in Å), the effective atomic charges Q (in e) and the bond populations P between nearest Me-O atoms (in e) for the ZrO_2-terminated $CaZrO_3$ (001) surface. Positive (negative) values refer to displacements in the direction outwards (inwards) the surface

ZrO_2-terminated $CaZrO_3$ (001) surface			
Layer no.	Ion	Property	B3LYP
1	Zr	D	−0.054
		Q	+2.172
		P	+0.102
	O	D	−0.096
		Q	−1.258
		P	+0.018
2	Ca	D	+0.176
		Q	+1.772
		P	+0.012
	O	D	+0.052
		Q	−1.235
		P	+0.090
3	Zr	D	−0.002
		Q	+2.14
		P	+0.098
	O	D	−0.00368
		Q	−1.286
		P	+0.014

Table 7
Calculated absolute magnitudes of atomic displacements D (in Å), the effective atomic charges Q (in e) and the bond populations P between nearest Me-O atoms (in e) for the CaO-terminated $CaZrO_3$ (001) surface. Positive (negative) values refer to displacements in the direction outwards (inwards) the surface

CaO-terminated $CaZrO_3$ (001) surface			
Layer no.	Ion	Property	B3LYP
1	Ca	D	−0.416
		Q	+1.763
		P	+0.024
	O	D	−0.033
		Q	−1.443
		P	+0.050
2	Zr	D	+0.046
		Q	+2.186
		P	+0.072
	O	D	+0.00036
		Q	−1.353
		P	+0.012
3	Ca	D	−0.108
		Q	+1.781
		P	+0.016
	O	D	−0.02
		Q	−1.318
		P	+0.092

Δd_{23}. The inward relaxation of the Ca atom (10.01% of a_0) is much larger than that of oxygen atom (0.79% of a_0) for the CaO-terminated $CaZrO_3$ (001) surface, which leads to a considerable rumpling of the outermost plane (see Table 5). The amplitude of surface rumpling of the CaO-terminated $CaZrO_3$ (001) surface (9.22) is predicted to be more than nine times larger than that for ZrO_2-terminated $CaZrO_3$ (001) surface.

Atomic displacements, the effective static charges, and bond populations between nearest metal and oxygen atoms are give in Tables 6 and 7. The major effect observed there is strengthening of the Zr-O chemical bond covalency near the ZrO_2-terminated $CaZrO_3$ (001) surface. Note that Zr and O effective charges in the $CaZrO_3$ bulk (+2.144e and −1.310e, respectively) are much smaller than those expected in an ionic model (+4.00e and −2.00e, respectively). The Zr-O bond in the $CaZrO_3$ is considerably

Table 8
Calculated cleavage, relaxation, and surface energies for $CaZrO_3$ (001) surfaces (in electron volt per surface cell)

Surface	Termination	$E_{(cl)}$	$E_{(rel)}$	$E_{(surf)}$
$CaZrO_3$ (001)	CaO-term.	1.54	−0.67	0.87
	ZrO_2-term.	1.54	−0.21	1.33

Table 9
Calculated optical band gap for $CaZrO_3$ bulk, as well as for CaO and ZrO_2-terminated (001) surfaces. Calculation and experimental results of other authors for $CaZrO_3$, $SrZrO_3$ and $BaZrO_3$ band gaps are listed for comparison

Termination	$CaZrO_3$ gap B3LYP	$CaZrO_3$ gap GGA [6]	$CaZrO_3$ gap LDA [6]	$SrZrO_3$ gap B3LYP [19]	$BaZrO_3$ gap B3LYP [5]
Bulk	5.40	3.315	3.283	5.31 [19]	4.79 [5]
Bulk (Exp.)	–	–	–	5.6 [49]	5.00 [50]
AO-term. (001)	5.00	3.106	2.913	5.04	–
BO_2-term. (001)	5.22	2.967	2.827	4.91	–

populated (+0.086*e*). The Zr-O bond population for the ZrO_2-terminated $CaZrO_3$ (001) surface is (+0.102*e*) (see Table 6), which is considerably larger than the relevant value in the bulk. In contrast, the Ca-O bond populations are very small. This effect is also well seen from the Ca effective charge, which is close to the formal ionic charge of +2.00*e*.

The results of calculations for the surface, cleavage and relaxation energies of CaO and ZrO_2-terminated $CaZrO_3$ (001) surfaces are presented in Table 8. According to my calculations the relaxation energy for CaO-terminated $CaZrO_3$ (001) surface (−0.67 eV) is considerably larger than the relaxation energy for ZrO_2-terminated $CaZrO_3$ (001) surface (−0.21 eV), which leads to large differences in surface energies. My calculated surface energies for the CaO and ZrO_2-terminated $CaZrO_3$ (001) surfaces are 0.87 eV and 1.33 eV, respectively.

My B3LYP calculated $CaZrO_3$ optical bulk band gap is 5.40 eV (see Table 9). The $CaZrO_3$ bulk band gap calculated by Brik *et al*. [6] using GGA (3.315 eV) and LDA (3.283 eV) is by a factor of 1.6 smaller than my B3LYP result (5.40 eV). It seems reasonable ratio between B3LYP result from one side, as well as GGA and LDA results from another side, since it is well known that the local-density and generalized-gradient approximations to density functional theory systematically underestimate the band gap in ABO_3 perovskites and another materials; an error of a factor of 1.5 is typical [2]. My B3LYP calculated optical band gap for the CaO- and ZrO_2-terminated $CaZrO_3$ (001) surfaces becomes smaller with respect to the bulk optical band gap. Also according to the GGA and LDA calculations performed by Brik et al. [6], the $CaZrO_3$ band gap near the (001) surfaces is reduced with respect to the bulk value approximately by 0.2–0.4 eV (see Table 9).

IV. Conclusions

According to the results of my calculations, all upper and third layer atoms for CaO- and ZrO_2-terminated $CaZrO_3$ (001) surfaces relax inwards, whereas all second layer atoms relax upwards. Such relaxation pattern is typical for ABO_3 perovskite (001) surfaces [2]. In (001) surface, the displacement of upper layer Ca atom on the CaO-terminated surface is more than seven times larger than that of upper layer Zr atom on the ZrO_2-terminated $CaZrO_3$ (001) surface. The surface rumpling for CaO-terminated $CaZrO_3$ (001) surface is more than nine times larger than for the ZrO_2-terminated $CaZrO_3$ (001) surface. My calculations for the $CaZrO_3$ (001) surfaces predict a compression of the distance between the first and second planes, and an expansion for the second and third planes. My *ab initio* calculations indicate a considerable increase of the Zr-O chemical bond covalency

(0.102*e*) near the ZrO_2-terminated $CaZrO_3$ (001) surface relative to the $CaZrO_3$ bulk (0.086*e*).

B3LYP calculated CaO (0.87 eV) and ZrO_2-terminated (1.33 eV) $CaZrO_3$ (001) surface energies are considerably smaller than another ABO_3 perovskite polar (011) surface energies [2]. Finally, the ABO_3 perovskite (111) surfaces are always energetically most unfavourable and unstable surfaces according to all performed calculations [5, 51]. My current $CaZrO_3$ (001) surface energy calculation results are in a good agreement with the previous calculation results dealing with $CaZrO_3$ (001) surface energies performed earlier by Brik *et al*. [6]. For example, also from both LDA and GGA calculations by Brik *et al*. [6] follows, that the CaO-terminated $CaZrO_3$ (001) surface energy is considerably smaller than the ZrO_2-terminated $CaZrO_3$ (001) surface energy. The calculated optical band gaps near the CaO- and ZrO_2-terminated $CaZrO_3$ (001) surfaces are considerably reduced with respect to the bulk band gap. This finding is in line with the narrowing of the band gap at $SrZrO_3$ and $PbZrO_3$ (001) surfaces reported earlier by Eglitis and Rohlfing [19].

Funding

This work was supported by the Latvian Council of Science Grant No. 374/2012 and ESF Grant No. 2013/0046/1DP/1.1.1.2.0/APIA/VIAA/021.

References

1. M. Dawber, K. M. Rabe, and J. F. Scott, Physics of thin-film ferroelectric oxides. *Rev. Mod. Phys.* **77**, 1083–1130 (2005).
2. R. I. Eglitis, *Ab initio* calculations of $SrTiO_3$, $BaTiO_3$, $PbTiO_3$, $CaTiO_3$, $SrZrO_3$, $PbZrO_3$ and $BaZrO_3$ (001), (011) and (111) surfaces as well as F centers, polarons, KTN solid solutions and Nb impurities therein. *Int. J. Mod. Phys. B.* **28**, 1430009 (2014).
3. J. F. Scott, *Ferroelectric Memories*. Springer: Berlin; (2000).
4. R. E. Cohen, Origin of ferroelectricity in perovskite oxides. *Nature*. **358**, 136–138 (1992).
5. R. I. Eglitis, *Ab initio* calculations of the atomic and electronic structure of $BaZrO_3$ (111) surfaces. *Solid State Ionics.* **230**, 43–47 (2013).
6. M. G. Brik, C. G. Ma, and V. Krasenko, First-principles calculations of the structural and electronic properties of the cubic $CaZrO_3$ (001) surfaces. *Surf. Sci.* **608**, 146–153 (2013).
7. E. Blokhin, R. A. Evarestov, D. Gryaznov, E. A. Kotomin, and J. Maier, Theoretical modelling of antiferrodistortive phase transition for $SrTiO_3$ ultrathin films. *Phys. Rev. B.* **88**, 241407(R) (2013).
8. R. I. Eglitis and D. Vanderbilt, First-principles calculations of atomic and electronic structure of $SrTiO_3$ (001) and (011) surfaces. *Phys. Rev. B.* **77**, 195408 (2008).
9. N. Erdman, K. R. Poeppelmeier, M. Asta, O. Warschkow, D. E. Ellis, and L. D. Marks, The structure and chemistry of the TiO_2-rich surface of $SrTiO_3$ (001). *Nature*. **419**, 55–57 (2002).
10. E. Heifets, R. I. Eglitis, E. A. Kotomin, J. Maier, and G. Borstel, *Ab initio* modeling of surface structure for $SrTiO_3$ perovskite crystals. *Phys. Rev. B.* **64**, 235417 (2001).
11. A. M. Kolpak, D. Li, R. Shao, A. M. Rappe, and D. A. Bonnell, *Phys. Rev. Lett.* **101**, 036102 (2008).
12. R. I. Eglitis and D. Vanderbilt, *Ab initio* calculations of the atomic and electronic structure $CaTiO_3$ (001) and (011) surfaces. *Phys. Rev. B.* **78**, 155420 (2008).
13. A. Hofer, M. Fechner, K. Duncker, M. Holzer, I. Mertig, and W. Widdra, Persistence of surface domain structures for a bulk ferroelectric above T-C. *Phys. Rev. Lett.* **108**, 087602 (2012).
14. E. A. Kotomin, R. I. Eglitis, J. Maier, and E. Heifets, Calculations of the atomic and electronic structure for $SrTiO_3$ perovskite thin films. *Thin Solid Films*. **400**, 76–80 (2001).

15. C. Bungaro and K. M. Rabe, Coexistence of antiferrodistortive and ferroelectric distortions at the $PbTiO_3$ (001) surface. *Phys. Rev. B.* **71**, 035420 (2005).
16. J. M. Zhang, J. Cui, K. W. Hu, V. Ji, and Z. Y. Man, Ab initio modelling of $CaTiO_3$ (110) polar surfaces. *Phys. Rev. B.* **76**, 115426 (2007).
17. R. I. Eglitis, G. Borstel, E. Heifets, S. Piskunov, and E. Kotomin, *Ab initio* calculations of the $BaTiO_3$ (100) and (110) surfaces. *Journal of Electroceramics*. **16**, 289–292 (2006).
18. R. I. Eglitis, First-principles calculations of $BaZrO_3$ (001) and (011) surfaces. *J. Phys.: Condens. Matter.* **19**, 356004 (2007).
19. R. I. Eglitis and M. Rohlfing, First-principles calculations of the atomic and electronic structure of $SrZrO_3$ and $PbZrO_3$ (001) and (011) surfaces. *J. Phys.: Condens. Matter.* **22**, 415901 (2010).
20. E. A. Kotomin, S. Piskunov, Y. F. Zhukovskii, R. I. Eglitis, A. Gopejenko, and D. E. Ellis, The electronic properties of an oxygen vacancy at ZrO_2-terminated (001) surfaces of a cubic $PbZrO_3$: computer simulations from the first principles. *Phys. Chem. Chem. Phys.* **10**, 4258–4263 (2008).
21. G. Borstel, R. I. Eglitis, E. A. Kotomin, and E. Heifets, Modelling of defects and surfaces in perovskite ferroelectrics. *Phys. Stat. Sol. B.* **236**, 253–264 (2003).
22. E. A. Kotomin and A. I. Popov, Radiation-induced point defects in simple oxides. *Nuclear Instruments and Methods in Physics Research Section B.* **141**, 1–15 (1998).
23. E. A. Popov A. I., Kotomin, and J. Maier, Basic properties of the *F*-type centers in halides, oxides and perovskites. *Nuclear Instruments and Methods in Physics Research Section B*. 2010; **268**, 3084–3089.
24. I. Colera, E. Gonzalez, E. Soria, J. L. De Segovia, E. L. Ronam, and Y. Chen, Electron simulated desorption study of the MgO (100) – D_2O system. *Journal of Vacuum Science & Technology A.* **15**, 1698–1703 (1997).
25. O. I. Aksimentyeva, V. P. Savchyn, V. P. Dyakonov, S. Piechota, Y. Y. Horbenko, I. Y. Opainych, P. Y. Demchenko, A. I. Popov, and H. Szymczak, Modification of polymer-magnetic nanoparticles by luminescent and conductiong substances. *Mol. Cryst. Liq. Cryst.* **590**, 35–42 (2014).
26. O. Aksimentyeva, V. Savchyn, I. Opaynych, P. Demchenko, Y. Horbenko, V. Pankratov, and A. I. Popov, Effects of polymer matix on the structure and luminescence properties of barium zirconate nanocrystals. Chem. *Metall Alloys*. **6**, 177–182 (2013).
27. N. Bickel, G. Schmidt, K. Heinz and K. Müller, Ferroelectric relaxation of the $SrTiO_3$ (100) surface. *Phys. Rev. Lett.* **62**, 2009–2011 (1989).
28. T. Hikita, T. Hanada, M. Kudo, and M. Kawai, Structure and electronic state of the TiO_2 and SrO terminated $SrTiO_3$ (100) surfaces. *Surf. Sci.* **287–288**: 377–381 (1993).
29. A. Ikeda, T. Nishimura, T. Morishita, and Y. Kido, Surface relaxation and rumpling of TiO_2-terminated $SrTiO_3$ (001) determined by medium energy ion scattering. *Surf. Sci.* **433–435**, 520–524 (1999).
30. G. Charlton, S. Brennan, C. A. Muryn, R. McGrath, D. Norman, T. S. Turner, and G. Thorthon, Surface relaxation of $SrTiO_3$ (001). *Surf. Sci.* **457**, L376–L380 (2000).
31. P. A. W. Heide, Q. D. Jiang, Y. S. Kim, and J. W. Rabalais, X-ray photoelectron spectroscopic and ion scattering study of the $SrTiO_3$ (001) surface. *Surf. Sci.* **473**, 59–70 (2001).
32. W. Maus-Friedrichs, M. Frerichs, A. Gunhold, S. Krischok, V. Kempter, and G. Bihlmayer, The characterization of $SrTiO_3$ (001) with MIES, UPS(Hel) and first-principles calculations. *Surf. Sci.* **515**, 499–506 (2002).
33. V. R. Saunders, R. Dovesi, C. Roetti, M. Causa, N. M. Harrison, R. Orlando, and C. M. Zicovich-Wilson, CRYSTAL-2006 User Manual. University of Torino. Torino, Italy; (2006).
34. R. E. Cohen, Periodic slab LAPW computations for ferroelectric $BaTiO_3$. *J. Phys. Chem. Solids*. **57**, 1393–1396 (1996).
35. R. E. Cohen, Surface effects in ferroelectrics: Periodic slab computations for $BaTiO_3$. *Ferroelectrics*. **194**, 323–342 (1997).
36. S. Piskunov, E. Heifets, R. I. Eglitis, and G. Borstel, Bulk properties of $SrTiO_3$, $BaTiO_3$ and $PbTiO_3$ perovskites: an *ab initio* HF/DFT study. *Comput. Mater. Sci.* **29**, 165–180 (2004).

37. H. Shi, R. Jia, and R. I. Eglitis, First-principles simulations on the aggregation of *F* centers in BaF_2: R centers. *Solid State Ionics*. **187**, 1–7 (2011).
38. H. Shi, R. Jia, and R. I. Eglitis, First-principles calculations of surface *H* centers in BaF_2. *Phys. Rev. B.* **81**, 195101 (2010).
39. L. Yue, R. Jia, H. Shi, X. He, and R. I. Eglitis, First-principles calculations for the *H* center in SrF_2 crystals. *J. Phys. Chem A.* **114**, 8444–8449 (2010).
40. H. Shi, R. I. Eglitis, and G. Borstel, *Ab initio* calculations of the hydrogen centres in CaF_2 and BaF_2. *J. Phys.: Condens. Matter.* **19**, 056007 (2007).
41. H. Shi, L. Chang, R. Jia, and R. I. Eglitis, *Ab initio* calculations of hydroxyl impurities in CaF_2. *J. Phys. Chem. C.* **116**, 6392–6400 (2012).
42. H Shi, L Chang, R Jia, and R. I. Eglitis. *Ab initio* calculations of the transfer and aggregation of *F* centers in CaF_2. *J. Phys. Chem. C.* 2012; **116**, 4832–4839.
43. A. D. Becke, Density-functional thermochemistry. 3. The role of exact exchange. *J. Chem. Phys.* **98**, 5648–5652 (1993).
44. C. Lee, W. Yang, and R. G. Parr, Development of the Colle-Salvetti correlation-energy formula into a functional of the electron density. *Phys. Rev. B.* **37**, 785–789 (1988).
45. H. J. Monkhorst and J. D. Pack, Special points for Brillouin-zone integrations. *Phys. Rev. B.* **13**, 5188–5192 (1976).
46. A. Rabenau, Perowskit und Fluoritphasen in den systemen ZrO_2-$LaO_{1,5}$-MgO und ZrO_2-$LaO_{1,5}$-CaO. *Z. Anorg. Allg. Chem.* **288**, 221–234 (1956).
47. C. R. A. Catlow and A. M. Stoneham, Ionicity in solids. *J. Phys. C: Solid State Phys.* **16**, 4321–4338 (1983).
48. R. C. Bochicchio and H. F. Reale, On the nature of crystalline bonding: extension of statistical population analysis to two- and three-dimensional crystalline systems. *J. Phys. B: At. Mol. Opt. Phys.* **26**, 4871–4883 (1993).
49. Y. S. Lee, J. S. Lee, T. W. Noh, D. Y. Byun, K. S. Yoo, K. Yamaura, and E. Takayama-Muromachi, Systematic trends in the electronic structure parameters of the 4d transition-metal oxides SrMO3 (M=Zr, Mo, Ru and Rh). *Phys. Rev. B.* **67**, 113101 (2003).
50. O. Fursenko, J. Bauer, G. Lupina, P. Dudek, M. Lukosius, C. Wenger, and P. Zaumseil, Optical properties and band gap characterization of high dielectric constant oxides. *Thin Solid Films*. **520**, 4532–4535 (2012).
51. R. I. Eglitis, Ab initio calculations of $BaTiO_3$ (111) surfaces. *Phase Transitions*. **86**, 1115–1120 (2013).